HHS Public Access

Author manuscript

Cell Rep. Author manuscript; available in PMC 2020 June 20.

Published in final edited form as:

Cell Rep. 2020 May 26; 31(8): 107668. doi:10.1016/j.celrep.2020.107668.

JARID1a Ablation in the Liver Alters Systemic Metabolism and Adaptation to Feeding

Kacee Ann DiTacchio[1,3], **Diana Kalinowska**[1,3], **Anand Rajamani Saran**[1], **Ashley Byrne**[2], **Christopher Vollmers**[2], **Luciano DiTacchio**[1,4,*]

[1]Department of Pharmacology, Toxicology, and Therapeutics, University of Kansas Medical Center, Kansas City, KS 66101, USA

[2]Department of Biomedical Engineering, University of California-Santa Cruz, Santa Cruz, CA 95064, USA

[3]These authors contributed equally

[4]Lead Contact

Graphical Abstract

[*]Correspondence: lditacchio@kumc.edu.

AUTHOR CONTRIBUTIONS

K.A.D. designed the study, carried out the research, analyzed and interpreted results, and wrote the manuscript; D.K. carried out the research and analyzed data; A.R.S. performed experiments; A.B. performed experiments; C.V. performed experiments, analyzed data, and reviewed the manuscript; and L.D. designed the study, carried out research, analyzed and interpreted results, wrote and reviewed the manuscript, and is responsible for the integrity of the work.

DECLARATION OF INTERESTS

The authors have no competing interests.

SUPPLEMENTAL INFORMATION

Supplemental Information can be found online at https://doi.org/10.1016/j.celrep.2020.107668.

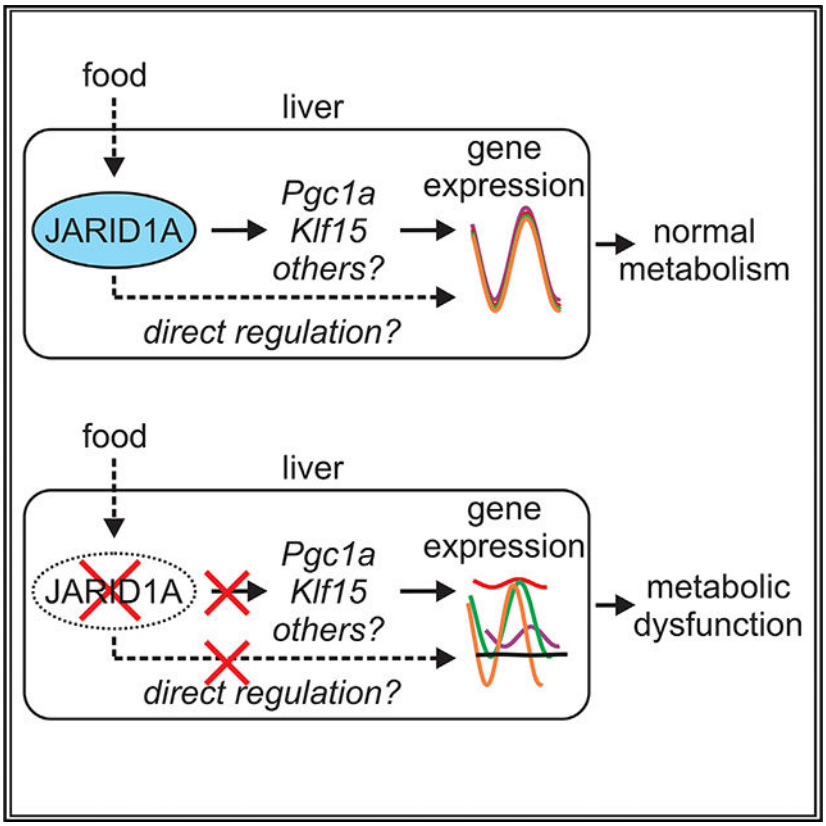

SUMMARY

The liver is a key regulator of systemic energy homeostasis whose proper function is dependent on the circadian clock. Here, we show that livers deficient in the oscillator component JARID1a exhibit a dysregulation of genes involved in energy metabolism. Importantly, we find that mice that lack hepatic JARID1a have decreased lean body mass, decreased respiratory exchange ratios, faster production of ketones, and increased glucose production in response to fasting. Finally, we find that JARID1a loss compromises the response of the hepatic transcriptome to nutrient availability. In all, ablation of hepatic JARID1a disrupts the coordination of hepatic metabolic programs with whole-body consequences.

In Brief

Feeding cues are a key driver of circadian rhythms in hepatic transcription. DiTacchio et al. report that JARID1a plays an important role in the liver transcriptional response to feeding. They show that its absence results in disruption to circadian gene expression in the liver with systemic consequences.

INTRODUCTION

The circadian clock is an endogenous timing mechanism that generates ~24-h behavioral and physiological oscillations that allow organisms to adapt to the changing environment inherent to the day-night cycle. In recent years, the circadian oscillator has emerged as a

critical orchestrator of metabolism and energy homeostasis with important implications to human health. Circadian dysfunction due to environmental factors commonly found in modern lifestyles has been linked to weight gain, metabolic syndrome, and diabetes (Albrecht, 2012; Bass and Takahashi, 2010; Feng and Lazar, 2012; Green et al., 2008). Critically, one way in which a high-fat, western-style diet promotes imbalance in energy metabolism is through the interference of circadian function (Kohsaka et al., 2007; Marcheva et al., 2010). Conversely, improvement of the circadian function via feeding-schedule manipulation is able to prevent and reverse the deleterious effects of high-fat diet (HFD) in mice (Chaix et al., 2014; Hatori et al., 2012), underscoring the importance of the circadian system in the maintenance of metabolic homeostasis.

At the molecular level, circadian rhythms originate from a cell-autonomous molecular circuit that impinges on physiology largely through transcriptional control. In mammals, these cell-autonomous oscillators are assembled into tissue-level oscillators that generate local rhythms in physiology. In the liver, the local oscillator is critical for normal function, and its disruption is associated with fatty liver, disruption of glucose homeosta sis, and diabetes (Feng et al., 2011; Lamia et al., 2008; Tahara and Shibata, 2016). Interestingly, the hepatic clock is required but not sufficient to generate large-scale transcriptional rhythms. Rather, the hepatic circadian transcriptome arises from an interaction between feeding-derived cues and the circadian clock (Vollmers et al., 2009). Although much progress has been made to understand the mechanisms underlying this interaction (Benegiamo et al., 2018; Greenwell et al., 2019; Kalvisa et al., 2018; Mange et al., 2017; Yeung et al., 2018), these remain to be fully defined, especially in terms of epigenetic regulators.

We previously identified the JmjC and AT-rich interacting domain protein 1a (JARID1a) as a non-redundant, evolution-arily conserved component of the circadian molecular machinery (DiTacchio et al., 2011). Mechanistically, JARID1a acts as a transcriptional co-activator for CLOCK-BMAL1 by inhibition of HDAC1 activity, acting as a molecular switch that triggers the transition from the repressive to the active phase of the circadian transcriptional cycle, and in its absence the amplitude of circadian oscillations is severely dampened and the period shortened. In addition, JARID1a has also been found to associate with and participate in the regulation by several transcription factors that have mechanistic links to energy metabolism (Benevolenskaya et al., 2005; Chan and Hong, 2001; Hayakawa et al., 2007). These observations, coupled to its role in the clock, led us to assess the role of JARID1a as a contributor of circadian regulation of energy metabolism *in vivo*.

RESULTS

Hepatic Deletion of Jarid1a Impacts Systemic Metabolism

We generated a *Jarid1a* liver-specific knockout (*Jarid1a*^{LKO}) mouse model to determine whether JARID1a plays a role at the intersection of circadian and systemic metabolic control in the liver, without confounding disruptions to behavioral rhythms. As expected, *Jarid1a*^{LKO} mice exhibited normal diurnal and circadian rhythms in activity and feeding, and unaltered caloric intake (Figures 1A–1E and S1A). From 10 weeks of age until the end of the study, we observed that *Jarid1a*^{LKO} mice exhibited a slight, but statistically significant, lower body weight than that of control mice ($p < 0.05$, $n = 20–24$ per group; Figure 1F). This

difference in body weight was accentuated under a HFD (40% kcal from fat), ($p < 0.002$, n = 19–25 per group; Figure 1F).

As measured in an intraperitoneal glucose tolerance test (GTT), *Jarid1a*^{LKO} mice fed a normal chow diet had normal glucose tolerance, but hepatic JARID1a-null mice showed exacerbation of HFD-induced glucose intolerance despite lower weight gain. (Figure 1G). Since the liver plays an important role in maintenance of blood glucose levels, we additionally performed a pyruvate tolerance test (PTT) to measure glucose production by the liver. On both standard and HFDs, *Jarid1a*^{LKO} mice exhibited an increased glucose response and total glucose output upon pyruvate challenge (Figures 1H and S1B). This suggests that *Jarid1a*^{LKO} mice may have increased gluconeogenesis; however, such heightened glucose production was insufficient to generate an overt diabetic phenotype in the present study, as no insulin resistance was detected (Figure S1C).

To understand the basis for the *Jarid1a*^{LKO} phenotype, we then focused on the liver of animals fed normal chow. Assessment of two key metabolic pathways involved in regulation of nutrient homeostasis, the mTOR and AMPK pathways, revealed no difference between genotypes, reflecting the unaltered feeding and behavioral rhythms in these animals and indicating inputs to the liver and their associated signaling remain intact (Figures S1D and S1E).

Transcriptomic Analysis of *Jarid1a*^{LKO} Livers Shows Dysregulated Metabolic Gene Expression

We next investigated the impact of JARID1a loss on the hepatic transcriptome via RNA sequencing (RNA-seq). To this end, we obtained a circadian mRNA timeline from livers harvested every 3 h (n = 3 mice/time point/genotype) from either control or JARID1a liver-specific null animals. In the resulting dataset we found that the effect in the oscillations of clock components upon ablation of JARID1a was modest, with the most noticeable effects being 3-h phase advances of *Cry1* and *Per2 mRNA*, a phase delay and slight increase in the global levels of *Cry2*, a change of *Fbxl3* from a ~24- to a ~12-h oscillation (Figure S2A; Data S1 $q = 0.044$), and an increase in the maximum levels of *Nr1d1* and *Bmal1* (Figure S2A). In addition, we found circadian occupancy of JARID1a at key CLOCK-BMAL1 binding regions in the *Cry1*, *Cry2*, and *Per2* promoters (Figure S2B), consistent with the previously described role of JARID1a as a regulator of CLOCK-BMAL1 transcription (DiTacchio et al., 2011).

Comparative analysis of over 9,000 transcripts present in both control and JARID1a-null datasets with the RAIN and JTK_CYCLE algorithms (Thaben and Westermark, 2014; Wu et al., 2016) identified 1,985 and 2,114 circadian genes in control livers and JARID1a-null livers, respectively, of which 1,150 oscillated in both datasets (Figure 2A; Data S1). Analysis of the common cyclers with DODR software (Thaben and Westermark, 2016) scored 395 transcripts as differentially rhythmic (Figure 2A; Data S1). In addition, in the absence of *Jarid1a*, 572 non-circadian genes had altered levels of expression ($q < 0.1$), 154 of which had absolute changes of at least 30% (Figure 2A; Data S1).

We classified genes that diverged between the *Jarid1a*$^{+/+}$ and *Jarid1a*^{LKO} hepatic transcriptomes and into one of four sets based on their expression profile (Groups 1–4; Figure 2A). Group 1 comprises transcripts whose expression was circadian only in *Jarid1a* $^{+/+}$ livers; Group 2 consists of transcripts that were rhythmic only in JARID1a-null livers; Group 3 comprises genes that oscillated in both datasets but with differential rhythmicity, and Group 4 consisted of non-circadian, differentially expressed genes. All of these sets were then subject to ontology analysis. In Group 1, we found enrichment of terms related to protein modification and signaling, energy metabolism ("lipid, fatty acid and cholesterol metabolism" and "other polysaccharide metabolism'') and nucleotide metabolism. Group 2 was dominated by genes related to cellular transport, but also included "cell cycle," "translation regulation," "amino acid metabolism," and "tumor suppressor." Group 3 and Group 4 were largely enriched for terms relating to energy homeostasis, with a clear tilt toward lipid metabolism (Figure S2C).

Genes that are affected in *Jarid1a*^{LKO} mouse livers include mRNAs of key genes involved in carbohydrate metabolism (Figures 2B and 2C), consistent with our observations in *Jarid1a*^{LKO}. For example, the transcript for PFKF1 exhibits circadian oscillations yet with an abnormal peak shape so that levels are reduced at circadian time 12 (CT12) when maximal feeding begins, and then has an accelerated drop in its levels (starting at CT21) compared to the control cohort. Although *Pfkfb1* participates in both gluconeogenesis and glycolysis, its expression is induced by a fed state (Zhao et al., 2012). We also found increased levels of pro-gluconeogenic genes, such as *Pck2*, whose gene product catalyzes a rate-limiting step in gluconeogenesis. Furthermore, *G6pc* mRNA, whose product catalyzes the last step in gluconeogenesis, was not determined by our bioinformatics analysis to fall into any of our four groups, but upon visual inspection, we noticed its expression levels elevated during the subjective day, with a significant difference between the two genotypes at CT27 and CT30 ($p < 0.05$). In JARID1a-deficient livers, expression of *Pgc1a,* a master regulator of energy metabolism that activates gluconeogenesis in part through induction of *G6pc,* exhibited ~50% higher overall levels ($q = 0.0055$). Specifically, *Pgc1a* levels were elevated at CT15, CT27, and CT30 (Figure 2D; $p < 0.05$). We performed chromatin immunoprecipitation (ChIP)-qPCR of the promoter region of PGC1a (Figure 2E) and found JARID1a occupancy at a cis-regulatory region containing a key cAMP response element (CRE) site that is also occupied by RNA polymerase II (RNA Pol II; Altarejos and Montminy, 2011; Herzig et al., 2001; Koike et al., 2012), which raises the possibility that JARID1a may influence gluconeogenesis indirectly through PGC1a, if at least in part.

We also found that the expression of the *Slc16a1* gene, which is responsible for transport of lactate across the plasma membrane, was scored as differentially rhythmic in JARID1a-null livers by DODR analysis ($p = 0.000117$). Closer analysis of *Slc16a1* levels shows increases at CT15 and decreased levels at CT21 and CT30 ($p < 0.05$), so that its expression has two peaks in a 24-h window. The most pronounced difference in *Slc16a1* between genotypes is during the early part of the active, feeding phase, which would be consistent with an increased capacity for lactate uptake, a key source of carbons used in glucose production; however, the timing of the disruption is such that the first peak in expression aligns with the active phase when mice are feeding, and glucose anabolism ordinarily would be minimal. JARID1a ablation also led to altered expression of the key components of the malate-

aspartate shuttle, which supplies oxaloacetate to the gluconeogenic pathway, so that either they lost circadian rhythmicity and showed elevated levels (*Got1*) or had altered circadian profiles (*Ogc/Slc25a11* and *Odc/Slc25a21*). Furthermore, we observed abnormalities in the expression of components of the tricarboxylic (TCA) cycle and the electron transport chain (*Sdhaf1, Atp5h, Atp5k*, and *Uqcrh*) in *Jarid1a*^{LKO} livers. However, despite previous reports implicating JARID1a in regulation in mitochondrial biogenesis in cultured cells (Lopez-Bigas et al., 2008), we found no difference in mitochondrial number in JARID1a-deficient livers (Figure S2D).

Jarid1a^{LKO} Mice Show Increased Lipid Use

JARID1a-null livers also exhibited decreased levels of genes involved in lipid transport (*Slc27a1*), accumulation (*Cidec*), increased lipid catabolism (*Bdh2*), as well as decreased levels of *Pparg* expression, a master lipogenesis regulator (Figure 2B). We next measured the diurnal respiratory exchange ratio (RER) of control and *Jarid1a*^{LKO} mice. During their active, feeding phase, normal mice have a higher RER, which is indicative of greater use of carbohydrates for fuel when these are plentiful, whereas their RER drops during their inactive phase, as fat stores are used to meet energetic demands (Figure 3A). In *Jarid1a*^{LKO} mice we found that a shift toward utilization of fatty acids exists during the active phase. It was interesting to find that ablation of hepatic JARID1a resulted in a detectable change in whole-body RER, given that neither activity nor feeding patterns are changed (Figures 1A–1D) and no genetic defect occurs outside the liver.

Comparison of the total serum triglyceride (TG) circadian profiles of control and *Jarid1a*^{LKO} mice was consistent with increased lipid use (Figure 3B). In control animals, serum TG levels first rise at CT15, as food consumed in the early night is digested, falling at the subjective day-to-night transition and then rise again as TGs enter the circulation as fasting progresses, peaking in the middle of the subjective day, and then declining as the active, feeding phase approaches. Although *Jarid1a*^{LKO} mice exhibit an initial increase in circulating TGs at CT15 similar to wild-type animals, their levels drop just 3 h later at CT18 and then rise again so that at CT21 their levels were almost double those of control mice (Figure 3B). Analysis of *Jarid1a*^{LKO} livers across the circadian cycle showed decreased levels of total TGs and several fatty acids (linoleic acid, palmitic acid, stearic acid, 1-monostearin, and 2-monoolein), as well as increased levels of glycerol, a major product of lipolysis and substrate of gluconeogenesis, and elevated 3-hydroxybutyrate content (Figure 3C). In addition, whereas a 24-h fast induces an influx of lipids to the wild-type liver exceeding the normal capacity for oxidation and resulting in measurable steatosis, we observed protection from fasting-induced steatosis in *Jarid1a*^{LKO} mice (Figures 3D and 3E).

In non-diabetic animals, the liver engages in *de novo* glucose production during periods of fasting in order to maintain blood glucose homeostasis, and in ketogenesis to supply the body with an alternative energy source. As our observations suggest that *Jarid1a*^{LKO} livers may have increased glucose production concomitant with lipid use, we examined the effects of fasting on blood glucose levels in *Jarid1a*^{LKO} versus control animals. In both groups, blood glucose remained at levels comparable to mice fed *ad libitum* (Figure S3A) up to 9 h following food removal. However, after fasting for 12 h, blood glucose levels in control mice

declined, whereas they remained elevated in *Jarid1a*^{LKO} mice even following 15 h without food (Figure 3F). Blood ketones were not detectable in animals fed *ad libitum* (not shown) or immediately after food removal (Figure 3G). Beginning at 3 h after food withdrawal, blood ketone levels remained indistinguishable between cohorts until 12 h after fasting, when the ketone concentration reached levels much higher in *Jarid1a*^{LKO} mice (Figure 3G). By 24 h, we could no longer observe a difference in blood glucose between genotypes, but blood ketone levels were still higher in mutant animals (Figures S3B and S3C). These results suggest that livers lacking JARID1a have an increased capacity to maintain glucose levels during the earlier stages of a fast and to generate ketones.

Abnormal Amino Acid Metabolism in Livers of *Jarid1a*^{LKO} Mice

JARID1a-null livers also exhibited alterations in the circadian expression of several genes linked to protein and amino acid catabolism (Figure 2B). Such alterations included elevation of genes involved in of alanine and aspartate metabolism (*Aspdh*), glutaminolysis (*Gls2*), glutamate metabolism (*Glud1*), histidine degradation (*Hal*), threonine catabolism (*Tha1*), amino acid transport (*Slc7a2*), and autophagy (*Atg7*, *Atg14*, and *Atg101)*. Consistent with increased amino acid catabolism, we found dysregulation in the expression of genes of key components of the urea cycle including *Asl* and *Ass1*. Based on this latter observation, we inspected the mRNA expression of the key urea cycle genes *Cps1* and *Otc*. First, we noted that global expression of *Cps1,* which codes for a rate-limiting step for entry of the urea cycle, was increased ~34% ($p = 0.02$, $q = 0.174$), attributable to heightened expression in the subjective night (CT12–CT18) and was rendered rhythmic with a period ~15 h ($q = 0.02722$). Second, although in contrast to previous reports we did not observe circadian oscillations in the levels of *Otc*, its expression in *Jarid1a*^{LKO} liver became ultradian ($q = 0.014$; Data S1), so that it was elevated during the middle of the subjective day (CT15–CT18) and the middle of the subjective night (CT27–CT30) (Figure 2B). Additionally, we found that JARID1a-deficient liver exhibited altered expression of *Klf15* (Figure 4A), an important regulator of amino acid metabolism and circadian coordination of the urea cycle (Jeyaraj et al., 2012; Takashima et al., 2010), raising the possibility that the observed dysregulation of amino acid metabolism and nitrogen detoxification genes could be explained by direct influence of JARID1a on the *Klf15* gene. To test this, we performed chromatin immunoprecipitations from mouse liver chromatin and found enrichment of JARID1a at a critical cis-regulatory region of important for control of the *Klf15* gene expression by the glucocorticoid receptor (GR) and by BMAL1 (Asada et al., 2011; Jeyaraj et al., 2012), implying that its dysregulation in mutant livers is related to absence of JARID1a (Figure 4B).

Analysis of amino acid levels in hepatic tissue across the circadian cycle revealed abnormalities consistent with our transcriptomic observations (Figure 4C). First, the levels and/or circadian profiles of several gluconeogenic amino acids were disrupted, including alanine and glutamine, which are major carbon sources for *de novo* glucose synthesis. In normal livers, we found that alanine levels were highest during the active phase, dropped in the early subjective day, rose again in the middle of the inactive phase, before once again declining to lowest levels in the late inactive phase. In contrast, hepatic alanine levels were clearly circadian in *Jarid1a*^{LKO} animals, but with maximum levels delayed 6 h, peaking at

the subjective night-subjective day transition and remaining elevated for the duration of the latter. Similarly, we observed that glutamine levels oscillated with a peak at the end of the active phase in control livers, while glutamine abundance was delayed in *Jarid1a*^{LKO} livers such that its levels remained elevated during the subjective day. In addition, aspartate, glutamate, glycine, serine, and threonine levels of control livers fluctuated with a pattern similar to that of alanine, with a primary peak in the middle of the subjective night, and a secondary peak in the middle of the subjective day. This profile was lost in the absence of JARID1a; instead, these amino acids exhibited elevated levels in the early subjective day. Furthermore, we observed that JARID1a deficiency altered hepatic urea levels such that it lost its circadian profile and gained a second peak that coincided with the period when amino acids were heightened in the mutant liver.

Previous findings have reported that increased hepatic amino acid catabolism increases glucagon secretion by pancreatic α-cells (Solloway et al., 2015). We thus measured plasma glucagon to determine if this multi-system crosstalk might be occurring in *Jarid1a*^{LKO} mice as well. We found that average circulating glucagon levels in 24-h-fasted *Jarid1a*^{LKO} mice were nearly double those of control animals; however, the results did not quite meet the cutoff for statistical significance (Figure 4D; $p = 0.071$). We also performed body composition analysis by Echo-MRI, which showed that the fat mass of *Jarid1a*^{LKO} mice was unaltered, but their total lean body mass was significantly decreased (control, 22.27 ± 0.42 g; *Jarid1a*^{LKO}, 19.57 ± 0.8 g, mean ± SEM; Figure 4E). Since muscle is the major source of amino acids used for hepatic glucose production, it is possible that hepatic dysregulation of energy metabolism leads to increased muscle catabolism and loss of lean mass, diversion of dietary protein to the liver at the expense of availability to the muscle, or a combination of both.

Jarid1a-Deficient Livers Show a Defective Transcriptional Response to Feeding

The changes we observed in *Jarid1a*^{LKO} livers were reminiscent of those observed in fasted mouse liver (Sokolović et al., 2008), in whose transcriptome there is increased gluconeogenic, lipolytic, and proteolytic gene expression. Since many metabolic genes are responsive to nutrient status, we wondered whether *Jarid1a*^{LKO} mice were presenting a fasted-like phenotype due to an inability to respond to nutrient availability. To test this possibility, we subjected mice to a 12-h fasting:12-h feeding paradigm for three days. After the last fasted phase, one cohort of each genotype was maintained under fasted conditions, and another was given access to food for 2 h. RNA derived from mouse livers of every cohort ($n = 5$ animals/genotype/feeding status) was sequenced and analyzed (Data S2).

The transition from fasting to feeding involves a general reprogramming of metabolism within the liver in which glucose production and lipid catabolic processes are no longer needed and glycolytic and assimilative processes become relevant; we found widespread dysregulation in this transition (Figure 5). In control livers, 386 genes were responsive to food ($q < 0.1$; Data S2). Of these, 145 genes (37.6% of the food-responder set) either failed to respond to food or did so abnormally in a *Jarid1a*^{LKO} background (Figure 5A; Data S2).

Among these, we found that glucokinase (*Gck*), an enzyme that is strongly induced by feeding and catalyzes the first step in glycolysis, failed to fully respond to nutrient

availability in *Jarid1a*^{LKO} livers (Figure 5A). On the other hand, *G6pc* and *Cpt1a*, which respectively catalyze the rate-limiting steps in gluconeogenesis and fatty acid β-oxidation, are not fully repressed upon refeeding (Figure 5A). These observations reveal dysfunction in *Jarid1a*^{LKO} livers in the ability to responsively segregate opposing metabolic processes upon feeding.

We used Ingenuity Pathway Analysis (IPA) software to identify enriched processes that involve the genes affected by JARID1a ablation (Figure 5B). The top canonical pathways identified, the two highest scoring were the BAG pathway and the unfolded protein response (UPR), both of which are processes involving handling of misfolded proteins. Transcription of protein folding genes is increased at the day-night and night-day transitions (Hughes et al., 2009), and the fasted-to-fed state transition acutely activates the UPR in wild-type animals to assist the reorganization characteristic of the metabolic switch (Deng et al., 2013). In *Jarid1a*^{LKO} livers, we found blunted induction of key UPR and related endoplasmic reticulum (ER)-associated degradation (ERAD) regulators *Edem1* and *Hspa5* (also known as *Grp78/Bip*), as well as *Manf*, *Pdia4*, *Uba5*, and *Vapb* (Figure 5A). Other pathways impacted by loss of *Jarid1a* included the NRF2-mediated oxidative stress response, which acts to offset oxidative stress that occurs in processes like cellular respiration and fatty acid oxidation, enrichment of GR signaling, and cholecystokinin/gastrin signaling—all of which are processes associated with food intake and nutrient availability. Similarly, IPA also predicted a network of nine genes involved in control of genes affected by JARID1a deficiency. These include UPR regulators ATF6 and XBP, key regulators of control of energy metabolism and energetic status (CREB1, FOXO1, and PPARA), and genes involved in influence of inflammation on hepatic metabolism (CEBPA, NFKIBA, SMAD3, and STAT3; Rui, 2014; Tornatore et al., 2012; Figure 5C).

Finally, we cross-analyzed food-responsive genes affected in *Jarid1a*^{LKO} livers with our circadian datasets. Genes present in both datasets were divided first into whether they were feeding-induced or feeding-repressed, and subsequently assigned into four groups according to whether their maximal expression in the circadian dataset was localized to the early-to-mid subjective night (CT12–CT15), mid-to-late subjective night (CT18–CT21), early-to-mid subjective day (CT24–CT27), and mid-to-late subjective day (C30–C33). In genes belonging to the food-induced set (Figure 5D), we found that food-induced genes with their expression maxima in the first half of the subjective night, as a group, have a biphasic pattern with peaks ~12-h apart that in mutant livers is much more disorganized and with lower levels. Intriguingly, food-induced genes that normally exhibit their highest levels from CT18–CT21, ~3 h after the major feeding bout has occurred, have their maxima delayed to the early subjective day in JARID1a-null livers. Similarly, the group of food-induced genes with highest expression levels in the late day (CT30–CT33) exhibits a moderate increase in levels in the middle of the subjective night, which is delayed to the early subjective day in mutant livers. In contrast, we found no difference between genotypes in either the pattern of the gene group with maxima at CT24–CT27, which is the time frame where food intake is at its lowest, or in food-repressed gene sets (Figure 5E). When considered together, these observations suggest that the dysregulation we observe in the JARID1a-null transcriptome may be based, in part, on a defective transcriptional response to nutrient availability (Figure 5F).

DISCUSSION

The liver is a major metabolic organ of the body, responsible for coordinating relevant responses to both predictable fluctuations and acute changes in energy availability and demand. In mammals, glycolysis, lipogenesis, and global protein synthesis generally coincide with the active period, when feeding takes place. Conversely, during the inactive, fasting phase, energy homeostasis is maintained via the use of internal energy stores generated during the feeding period, via glycogenolysis, lipolysis, ketogenesis, and proteolysis. However, the timing of these different processes is not just a broad temporal segregation to the active-inactive phases. Carbohydrate intake is preferred in the early active phase, with a switch in preference for protein and lipid toward the end of the active period (Tempel et al., 1989). Consistently, in numerous species including humans, glycolysis, and lipogenesis peak in the early active phase, while glycogenesis peaks in the late active phase (Doi et al., 2010; Ishikawa and Shimazu, 1980; Panda et al., 2002). Conversely, glycogenolysis occurs during the early part of the inactive phase, while lipolysis and gluconeogenesis peak at the end of the inactive phase, as glycogen stores decline. Also coinciding with this time, the process of autophagy exhibits a circadian rhythm with maximal function at the end of the inactive period (Ma et al., 2011) when preferred energy stores have been exhausted, thus providing amino acids for energy or glucose production.

In the liver, temporal orchestration of metabolism is accomplished in large part via the imposition of large-scale oscillations in transcription, including genes that code for regulators of rate-limiting steps of anabolic and catabolic pathways (Panda et al., 2002). Here, we find that deletion of JARID1a in mouse liver results in extensive rewiring of the hepatic transcriptome. In the absence of JARID1a, the expression of ~20% (395/1985) of circadian transcripts exhibit dysregulation in the phase and/or amplitude of their expression, and a further 35% (695/1985) lose their circadian profile. Simultaneously, loss of JARID1a led to a gain of rhythmicity in 757 genes that are not rhythmic in normal livers. As such, the total number of circadian oscillating genes in the livers of both phenotypes is comparable (1,985 in control versus 2,114 in *Jarid1a*^{LKO}). Yet, the resulting transcriptomic states are not equivalent. In many cases, the expression changes we observed lead to a situation where expression levels differ in a temporally discrete manner. For example, whereas the pro-gluconeogenic genes *Slc16a1* and *Got1*, and *Glud1*, which are involved in amino acid catabolism, have a clear circadian expression pattern with a single maximum, in mutant livers these genes show two peaks, so that their levels are increased at times when their expression is normally at their nadir (Figure 2B). In addition, the same end effect can occur as a consequence of phase advance (*Atg7*, *Klf15*, and *Odc/Slc25a21*), phase delay (*Tha1* and *Sdhaf1*), or increased levels/amplitude (*Aspdh*, *Atg14*, *Bdh2*, *Hal*, *Slc7a2*, and *Ogc/Slc25a11*) in genes that remain circadian in *Jarid1a*^{LKO} livers, and by gain of oscillations upon ablation of JARID1a (*Atg17*, *Aspdh*, and *Gls2*). JARID1a deficiency also causes changes in ~8% (572/6787) of non-circadian transcripts common to both genotypes ($q < 0.05$). For example, we noted heightened global levels of *Pck2* and *Pgc1a* (gluconeogenesis), *Ass1* (amino acid catabolism), and *Bdh2* (ketogenesis). In contrast, we found decreased expression of *Slc27a1*, *Cidec*, and *Pparg,* which are involved in lipid uptake and storage. In addition, several genes with affected expression levels but identified as non-circadian show

ultradian rhythms (e.g., *Atp5k*; Figure 2B; Data S1), and others show visually identifiable peaks roughly 12-h apart, albeit with low amplitude (*Atp5h* and *Uqcrh*; Figure 2B). Interestingly, although we found a similar number of ultradian genes (period 12–15 h, $q < 0.05$) in control (433 genes) and *Jarid1a*^{LKO} livers (443 genes), only a minority of these were common (74 genes; ~17%) to both genotypes (Data S1). As ultradian rhythms in liver arise from an interplay between the local circadian clock and feeding cues, such an effect underscores the importance of JARID1a in maintenance of proper phase of oscillations. Finally, we know that at least some genes escape detection of our bioinformatics screen due to the discrete nature of their defects; *G6pc* and *Cps1* both have at least two time points with significantly increased expression in *Jarid1a*^{LKO} livers, but overall do not score as altered in circadian pattern nor are these disruptions enough to rate the overall expression levels as changed.

Although important, the hepatic clock on its own only partly accounts for the large-scale transcriptional rhythms observed in the liver. In synergy with the clock, feeding cues drive a large component of oscillatory genes and also feedback to entrain the clock (Greenwell et al., 2019; Schibler et al., 2003; Vollmers et al., 2009). This synergistic system allows the liver to anticipate the predictable fluctuating energy demands of the body while also maintaining the ability to respond to acute feeding cues. Our data implicate JARID1a in both functions. First, our RNA-seq timeline revealed a predominant impact of JARID1a loss on genes with circadian patterns of expression that included genes representing major metabolic programs. Second, our fasted-refed experiment demonstrated the importance of JARID1a in the genomic response to feeding, with an incomplete transition to the fed-state gene-expression profile in *Jarid1a*^{LKO} livers.

The liver is a control hub for whole-body energy homeostasis and, therefore, substantial disruption to liver physiology can have whole-body consequences. Although the genetic defect in the present study was limited to the liver, we observed phenotypes impacting the whole body including reduced lean mass, lower RERs, and lower overall body weight. The precise mechanisms by which muscle loss occurs in hepatic JARID1a-null mice remain unclear, but one possibility is that this phenomenon is due at least in part to increased amino acid catabolism in the mutant liver that either triggers protein catabolism in muscle and/or diverts dietary amino acids away from the rest of the body. The decrease in the RER indicates increased utilization of fatty acids for energy, and occurred during the active, feeding period when carbohydrates are plentiful and should be the favored fuel source. *Jarid1a*^{LKO} animals, however, have delayed expression of food-responsive genes at this time and instead rely more heavily on fat for energy. We also observed a greater glucose response in our PTT (suggestive of increased gluconeogenesis), greater ability to maintain blood glucose levels during fasting, and increased expression of gluconeogenic genes. One possible explanation for these collective observations is that the *Jarid1a*^{LKO} liver is unable to fully respond to carbohydrate nutrients, catabolizes amino acids for production of new glucose, and fuels the process with fatty acids. Anabolism generally and *de novo* glucose specifically are energy-intensive processes and may account for the decreased body weight over time in *Jarid1a*^{LKO} animals as more energy is used up in the interconversion of macronutrients. We did not include the HFD for our full study; however, we did observe a more pronounced weight deficit in *Jarid1a*^{LKO} animals of that group. Since *Jarid1a*^{LKO}

animals make more use of fat for energy, one might expect a rescue of body weight with HFD, but this was not observed. However, since high-fat chow has decreased protein content as well as carbohydrate, less dietary protein is available to the JARID1a-null liver, which may exacerbate the inefficiency in macronutrient utilization.

In part, the functions of JARID1a may occur through control of the expression of key transcription factors. First, our data show presence of JARID1a at the *Pgc1a* gene promoter (Figure 2E). Levels of JARID1a occupancy at this site are circadian, with maximal abundance taking place at the time points that become elevated in *Jarid1a*^{LKO} livers. The same region has been shown to bind p-Ser5 RNA Pol II anti-phasic to our findings herein for JARID1a (Koike et al., 2012), which suggests a repressive role for JARID1a in *Pgc1a* transcription. Given that PGC1a promotes transcription of genes of key gluconeogenic factors (Besseiche et al., 2015), these observations are consistent with the idea that *Jarid1a*^{LKO} livers may have increased gluconeogenic potential. Second, we find JARID1a presence at a cis-regulatory region of the *Klf15* gene (Figure 4B) that has been shown to be bound by the GR and BMAL1, two factors known to interact with JARID1a (Chan and Hong, 2001; DiTacchio et al., 2011). JARID1a abundance at this site parallels that of BMAL1, reminiscent of what is observed in the *Per2* gene promoter (DiTacchio et al., 2011), as well as that of p-RNA Pol II. Yet, instead of an effect in the overall levels of *Klf15* transcript, we observe a shortened period length (control 22.5 h, mutant 21 h; Data S1), and an advance in its phase such that *Klf15* transcript levels reach a nadir at CT18 and begin to increase at CT21 in mutant liver, whereas in control liver the nadir doesn't occur until CT3 and the rise starts at CT6 (Figure 4A); thus, its abundance is effectively increased during the subjective day. Consistently, DODR analysis scored *Klf15* as differentially rhythmic with an adjusted $p = 7.4 \times 10^{-5}$ (Data S1). Notably, KLF15 is a master regulator of both the urea cycle and amino acid catabolism, and higher levels of its transcripts are congruent with the increased levels of urea and amino acids that we observe in the same time frame (Figure 4C). However, although JARID1a influence on the expression of *Pgc1a* and *Klf15* may account for some of the effects we see in JARID1a-null livers, a more-extensive network of transcription factors is likely to be involved. Indeed, upstream regulator analysis of food-responsive genes impacted by JARID1a ablation suggests the involvement of at least 10 other regulators, which perhaps is not surprising given the complexity by which energy metabolism is controlled. Precisely how JARID1a impacts the function of these and/or other regulators remains to be defined, and warrants further study.

Altogether, our results show that the clock component JARID1a is required for the liver to adapt to exogenous nutrient availability, which is critical for both local and systemic metabolic health. Moreover, the role of JARID1a in regulation of energy metabolism mirrors its role in the circadian clock, where it acts to facilitate the transition from the repressive to the active phase of circadian transcription (DiTacchio et al., 2011). Here, our data indicate that JARID1a facilitates the transition from the fasted to the fed phase of hepatic transcription. Finally, given that many genes in JARID1a-null liver retain rhythmicity but exhibit phase and/or amplitude defects, *Jarid1a*^{LKO} mice present a framework to understand how metabolic cues and the circadian clock integrate to generate and entrain tissue-level rhythms.

STAR★METHODS

RESOURCE AVAILABILITY

Lead Contact—Further information and requests for resources and reagents should be directed to and will be fulfilled by the Lead Contact, Luciano DiTacchio (lditacchio@kumc.edu).

Materials Availability—All mouse lines used in this study are available from Jackson Laboratory.

Anti-JARID1a antibody samples are available upon request.

Data and Code Availability—RNA-seq datasets generated in this study are included in this article and raw sequencing files are available at the Sequence Read Archive (SRA) under project numbers SRA:PRJNA626351 and SRA:PRJNA626368. The published article includes any code generated during this study

EXPERIMENTAL MODEL AND SUBJECT DETAILS

Animal use and housing—All animals were used in accordance to KUMC Institutional Animal Care and Use Committee (ACUP#2018–2470).

Liver-specific JARID1a null (animals were generated by breeding *Jarid1a*$^{loxP/loxP}$ mice (*B6.129S6(Cg)-Kdm5atm1Kael/J, The* Jackson Laboratories stock 008572) with a transgenic mouse line that specifically expresses CRE in the liver at high levels (Albumin promoter-driven CRE; B6.Cg-Speer6-ps1Tg(Alb-cre)21Mgn/J, Jackson Laboratories stock 003574). Specifically, our breeding approach consisted of mating *Jarid1a*$^{loxP/+;Cre+}$ (heterozygote LoxP;Cre+) males and *Jarid1a*$^{loxP/+;Cre+}$ (heterozygote LoxP;Cre+) females to generate *Jarid1a*$^{+/+;Cre+}$ (control) and *Jarid1a*$^{loxP/loxP;Cre+}$ (hepatocyte-specific Jarid1a null) animals.

Group-housed mice always consisted of a mix of control and mutant animals.

Mice used in experiments were housed in ventilated cages (Tecniplast IVC) with corn cob bedding (except where explicitly noted) under a 12h:12h Light-Dark cycle. An exception to this was the body weight tracking in regular chow or high-fat diet fed mice and associated tolerance tests, which due to space availability issues were housed in a shared room under 14h:10h light dark cycle.

METHOD DETAILS

Body weight measurements and high fat diet feeding—8-week-old Jarid1a^{LKO} and control male mice were group housed with *ad libitum* access to either standard (LabDiet 5K67) or a high-fat diet (40% kcal from fat, Tekla Custom Diets TD.88137). Mice were subjected to weekly whole-body weight measurements for 18 weeks.

Glucose, pyruvate, and insulin tolerance tests—Ten-to-14-week-old group-housed male mice were fasted for 16 h in cages with paper bedding. At the end of the fasted period,

the lateral tail vein was incised to allow for blood collection. Fasted blood glucose was measured (FreeStyle Lite) before injection and recorded. Each mouse was injected with either pyruvate (2 mg/g body weight), glucose (1mg/g body weight), or insulin (1U/mg body weight). Subsequent measurements were made by collecting blood from the cut site before and after injection to generate a time course.

Circadian activity recordings—Control and *Jarid1a*^{LKO} (10-to-14-week-old) male mice were housed individually in standard cages with a custom-made wire top lid, placed in a custom-made, ventilated, light-tight chamber where voluntary activity was recorded and analyzed with a BigBrother video monitoring system (Figures 1A and S1). Circadian recordings were performed following field standards. Briefly, animals were entrained to a 12h:12h light-dark cycle for two weeks after which they were released into for a darkness for a further three weeks. Recordings during dark conditions was performed under indirect infrared light. Circadian period estimates were calculated from three weeks of DD data with ClockLab, using the Chi-square periodogram.

Food consumption—10-to-14-week-old individually-housed male mice were entrained to a 12h:12h LD cycle in a light-tight chamber, were transferred to a Minimitter chamber (Colombus Instruments). Total daily food consumption and meal pattern analysis of mice under 12 h:12 h LD was done for three days (Figure 1D).

Metabolic cages—Following entrainment to a 12h:12h LD cycle in a light-tight chamber, individually housed mice were transferred to a Promethion metabolic cage system (Sable Systems International, Las Vegas, NV). Recordings of the respiratory exchange ratio of 10-to-14-week-old male animals was done for a total of 5 days under a 12h: 12h LD cycle. Simultaneously, activity was also analyzed by beam break recordings.

Body composition—Total lean and fat mass analysis of 10-to-14-week-old male animals was done in an EchoMRI-1100 (EchoMRI LLC, Houston, TX) instrument following the manufacturer's instructions.

Fasting blood glucose and ketones—To reduce intra-sample variability arising from naturally-occurring differences in consumption patterns in different mice, 10-to-14-week-old male mice were subjected to 12 h fasting: 12 h feeding paradigm for three days (Figure S4A) in cages with paper bedding. At the end of the third feeding period, food was removed and blood glucose and ketone in fasted mice were respectively monitored with a FreeStyle Lite blood glucose and with a NovaMax Plus Ketone meters. *Ad libitum* controls were handled identically to fasted cohorts but with continuous access to food.

Circadian liver timeline generation—Mice (10-to-14-week-old male animals) were housed in a homemade light-tight chamber where they were entrained to a 12h: 12h light-dark cycle for two weeks. Following entrainment mice were released into total darkness. Beginning 24 hours after lights were turned off 3 mice per genotype were removed from the chamber and killed at 3-hour intervals for 24 hours. Specifically, under dim, red light mice were quickly anesthetized with isofluorane, decapitated and the blood collected for sera

collection. Immediately after euthanasia the carcass was taken to a contiguous dissection room where livers were excised and flash frozen and stored in dry ice until further use.

Fasted-refeeding tissue harvesting—Ten-to-14-week-old male animals were individually housed in ventilated cages with paper bedding and subjected to a three-day 12h fasting: 12h feeding paradigm (Figure S4A). At the end of the third fasting period mice of each genotype were either maintained under fasting conditions or allowed access to food for two hours before being killed. Each cohort consisted of n = 5 mice.

Liver extract preparation and immunoblotting—Frozen livers were pulverized with a supercooled mortar and pestle. For each sample approximately 100 mg of powdered liver was added to 3 mL of ice-cold Tissue Lysis Buffer (20 mM Tris HCl pH 7.4, 100 mM NaCl, 0.5 mM EDTA, 5% glycerol, 1% Tween-20, 1% NP-40, 0.2% SDS supplemented with cOmplete protease inhibitor (Roche, available from Millipore Sigma) and PhosSTOP phosphatase inhibitor (Roche available from Millipore Sigma Cat. 4906845001) cocktails), pulse vortexed and immediately homogenized with a polytron homogenizer. The homogenized sample was incubated in wet ice for 10 minutes, centrifuged at 20,000 *g,* 4°C, for 20 minutes. The clarified supernatant was then aliquoted and flash frozen for storage until further use. A small aliquot for the clarified supernatant was used for total protein quantification with a BCA assay (Pierce BCA Assay Kit, Thermo Fisher Scientific Cat.23225).

For each homogenate a total of 20 μg was resolved by SDS-PAGE, transferred onto a PVDF membrane and immunoblotted with antibodies described in the key reagents section. Data capture of immunoblots was done with an Odyssey Fc imaging system (LiCOR Biosicences, Nebraska, USA).

Chromatin immunoprecipitation—Approximately 300 mg of pulverized liver was added to 4 mL of PBS containing 2 mM of EGS (ethylene glycol bis(succinimidyl succinate)) crosslinker (Thermo Fisher Scientific Cat. 21565), vortexed vigorously for 10 s and tumbled end-over-end at room temperature for 20 minutes. The samples were then pulse-centrifuged and the supernatant discarded. Four mL of PBS containing 1% formaldehyde were then added to the pellet, which was then vortexed vigorously for 10 s and then tumbled as before for 15 minutes. The tissue was pelleted by pulse centrifugation and after decanting the supernatant the crosslinking reaction was quenched by tumbling at room temperature in 4 mL of 1M Tris HCl pH 8.0. Next, the crosslinked tissue pellet was dounce-homogenized (15 strokes) on ice in ice-cold hypotonic buffer (10 mM Tris HCl [pH 8.0], 10 mM KCl, 0.5 mM MgCl2). The homogenized tissue was then centrifuged at 800 *g* for 5 minutes at 4°C, and the resulting supernatant discarded. The pellet was carefully resuspended in S1 buffer (0.25 M sucrose and 10 mM MgCl2), gently layered on a sucrose cushion S2 (0.88 M sucrose and 0.5 mM MgCl2), and centrifuged at 3,000 *g* for 10 minutes at 4°C. The supernatant was carefully discarded, and chromatin was prepared by lysing the pelleted nuclei with Chromatin Sonication Buffer (CSB) (50 mM Tris-HCl pH 8.0, 10 mM EDTA, 25% Glycerol, 1% SDS supplemented with c0mplete protease inhibitor (Roche) and PhosStop phosphatase inhibitor (Roche) cocktails), sonicated in an Epishear cuphorn sonicator to 300–500 bp fragments, and clarified by centrifugation at 20,000 *g,* 4°C, for 15

minutes. Total protein in clarified liver chromatin was quantified with a BCA assay, aliquoted and flash frozen for storage until further use.

For each individual immunoprecipitation a total of 200 μL of CSB containing 50 μg of sonicated (0.25 μg/μL) chromatin was diluted to 1.2 mL of Immunoprecipitation Buffer (20 mM Tris HCl pH8.0, 20 mM NaCl, 2 mM EDTA, 1% Triton X-100) supplemented with c0mplete protease inhibitor (Roche) and PhosStop phosphatase inhibitor (Roche) cocktails. Diluted samples were then precleared by incubation with 4 μg of rabbit IgG (ThermoFisher Scientific Cat # 02–6102) pre-bound to 25 μL of Protein G magnetic beads (Dynabeads, ThermoFisher Scientific, Cat. 10004D) tumbling end-over-end at 4°C, for 2 hours. After magnetic removal of the IgG-bead complex, an aliquot of the cleared chromatin was taken and set aside as an input sample. The precleared chromatin solution was incubated with 4 μg of anti-JARID1a (custom made, see STAR key material description) pre-bound to 25 μL of Protein G magnetic beads tumbling end-over-end at 4°C, for 12–18 hours. Following incubation, the magnetic beads were collected and washed for tumbling for five minutes at 4°C with each of the following buffers (all supplemented with protease and phosphate inhibitors as before) in the order listed:

1. 20 mM Tris HCl pH 8.0, 150 mM NaCl, 2 mM EDTA, 1% Triton X-100, 0.1% SDS.
2. 20 mM Tris HCl pH 8.0, 300 mM NaCl, 2 mM EDTA, 1% Triton X-100, 0.1% SDS.
3. 20 mM Tris HCl pH 8.0, 500 mM NaCl, 2 mM EDTA, 1% Triton X-100, 0.1% SDS.
4. 10 mM Tris HCl pH 8.0, 0.25 M LiCl, 1 mM EDTA, 1% Triton X-100, 1% Sodium deoxycholate.
5. TE buffer (10 mM Tris HCl pH 8.0, 1 mM EDTA).

Following the washing process, immunoprecipitated chromatin complexes were released from the antibodies by incubation for 20 minutes at 65°C in 500 μL of Elution Buffer (1% SDS, 0.1 M $NaHCO_3$). After magnetic removal of the antibody-bead complex, the eluted chromatin complexes were supplemented with 25 μL 5 M NaCl and incubated overnight (12 h) at 65°C to reverse the cross-link. The reverse-crosslinked solution was then supplemented with 20 μL 1 M Tris HCl pH 8.0 and 10 μL of 0.5 M EDTA pH 8.0, incubated first with 2 μg of RNase A at 37°C for 1 h, followed by incubation 2 μg of Proteinase K at 50°C. DNA was then extracted by phenol:chloroform extraction and ethanol precipitated in the presence of 10 μg of glycogen (ThermoFisher Scientific Cat. R0561). Recovered DNA was then resuspended in 150 μL of Molecular-grade water (Fisher Bioreagents Cat. BP561–1) and analyzed by QPCR using PerfeCTa SYBR Green FastMix (Quanta bio, Cat. 95072–05K) with the primers provided in the key resource table.

Custom rabbit anti-JARID1a antibody was raised against human JARID1a residues 1676–1690 by Pacific Immunology (Ramona, CA) and validated for its suitability for chromatin immunoprecipitation and immunoblot applications in wild-type and *Jarid1a*^{LKO} livers (Figures S4B and S4C)

mtDNA:nuclear DNA ratio via QPCR—The hepatic mitochondrial number estimates were calculated as the ratio of mitochondrial *Nd1*gene to nuclear-encoded *Hk2* gene. Liver DNA was isolated with DNAzol (Thermo Fisher Scientific Cat. 105032027) following the manufacturer's instructions. Quantification of mitochondrial and nuclear DNA content was done via QPCR with PerfeCTa SYBR Green FastMix (Quanta bio, Cat. 95072–05K) with primers provided in the resource table. Sequences of the primers were obtained from Quiros et al. (2017).

Metabolite analysis—Quantification of hepatic gluconeogenic amino acids and urea were performed by the Vanderbilt University Hormone Assay & Analytical Core via HPLC using a Biochrom 30 Amino Acid analyzer. Briefly, liver samples are weighed and homogenized in 3 volumes (volume: weight) of ice-cold 5-Sulfosalicylic Acid with a polytron homogenizer, followed by centrifugation at 3000 *g* at 4 C for 15 minutes. The volume of the clarified supernatant is measured and an aliquot is shipped to the core for quantification. The results are provided as concentrations, which are then used to calculate moles per tissue weight.

Hepatic triglycerides were analyzed via GC performed by the Lipid Core at Vanderbilt University on liver samples with data obtained as quantity per mg of tissue. Levels of specific lipids shown in Figure 3C were obtained from GC-TOF MS metabolite analysis performed by the NIH West Coast Metabolomics Center at UC Davis. Triglyceride levels in sera collected across the circadian cycle were measured with a Pointe Scientific, Inc. Triglyceride assay kit (Cat. T732–500) following the manufacturer's instructions.

Histology—Mice were either fasted for 24h or maintained with *ad libitum* access to food, sacrificed by cervical dislocation, and necropsied. For each cohort four different mice were used. Whole body weight was recorded, and liver tissue was collected. Liver sections were cryopreserved, sectioned with a cryostat, and stained with Oil red O.

RNaseq library preparation—RNA was extracted from control and *Jarid1a*^{LKO} pulverized liver samples from the circadian timeline and fasted-refeeding experiments using TRIzol reagent following the manufacturer's instructions. RNaseq libraries for each biological replicate were then constructed using a variation of the Smartseq2 method (Picelli et al., 2013). In short, for each biological replicate we generated cDNA from total RNA using the Smartscribe Enzyme (Clontech) and a oligo-dT primer modified with a universal priming site (ISPCR). During reverse transcription another universal priming site (ISPCR) was added at to the end of the cDNA corresponding to the 5′ end of transcripts through template switching to an additional oligo. The resulting full-length cDNA was treated with RNase A and Lambda Exonuclease to remove template-switch oligos and primer dimers, respectively and amplified using the universal priming sites with KAPA HIFI Hot Start Readymix (KAPA) and a ISPCR primer. The PCR product was then treated with Tn5 enzyme loaded with Tn5ME A/R and Tn5ME B/R adapters. The resulting fragments were amplified using Nextera A and Nextera B index primers using KAPA HIFI DNA Polymerase (KAPA), size selected to 350–800bp, and sequenced on an Illumina HiSeq 2500.

Nextera_A_Index_Primer, AATGATACGGCGACCACCGAGATCTACAC[i5]TCGTCGGCAGCGTCAGATG

Nextera_B_Index_Primer, CAAGCAGAAGACGGCATACGAGAT[i7]GTGGGCTCGGAGATGTGTAT

Tn5ME-R, [phos]CTGTCTCTTATACACATCT

Tn5ME-A (Illumina FC-121–1030), TCGTCGGCAGCGTCAGATGTGTATAAGAGACAG

Tn5ME-B (Illumina FC-121–1031), GTCTCGTGGGCTCGGAGATGTGTATAAGAGACAG

Smartseq2-TSO, AAGCAGTGGTATCAACGCAGAGTACATrGrGrG

OligodT/iMeCisodC/AAGCAGTGGTATCAACGCAGAGTACT30VN

ISPCR, AAGCAGTGGTATCAACGCAGAGT

RNA-seq data processing—Fastq files from the Illumina HiSeq2500 run aligned to GRCm38/mm10 version of the mouse genome using the STAR aligner (Dobin et al., 2013). Raw counts were normalized to counts per million (CPM). For the circadian timeline cutoff of expression was defined as CPM > = 1 in 41 out of the 48 libraries sequenced. Fasting-refeeding for each genotype expressed genes were defined as those with a CPM > = 1 in 6 out of the 10 libraries sequenced (5 fasted and 5 fed).

Rhythmicity analysis—To define circadian rhythmicity the dataset for each genotype was independently analyzed with JTK algorithm of the MetaCycle package (Wu et al., 2016) as well as with the RAIN circadian rhythmicity analysis package (Thaben and Westermark, 2014). Both of these algorithms are able to handle biological replicates and our data was so analyzed without concatenation.

MetaCycle analysis options used: time points = rep(seq(12, 33, by = 3), each = 3), minper = 18, maxper = 28, cycMethod = c("JTK"), analysisStrategy = "auto," outputFile = TRUE, outIntegration = "both," adjustPhase = "predictedPer," combinePvalue = "fisher," weightedPerPha = FALSE, ARSmle = "auto," ARSdefaultPer = 24, outRawData = FALSE, releaseNote = TRUE, outSymbol = ""

RAIN analysis options used: deltat = 3, period = 24, period.delta = 12, nr.series = 3, peak.border = c(0.3, 0.7), verbose = TRUE, method = 'independent'

For each genotype dataset the non-adjusted *p-value*s obtain by MetaCycle and RAIN were combined with Fisher's sumlog method and corrected for multiple comparisons with the Benjamini-Hochberg method to obtain a q-value. Circadian rhythmicity was defined as combined q < 0.05 with a period > = 18 and ≤ 28, with the MetaCycle-provided relative amplitude metric > 0.15. When assessing gain or loss of circadian rhythmicity, a gene was deemed to remain circadian if q < 0.05 with period > = 18 and ≤ 28 irrespective of relative amplitude score. Ultradian rhythmicity was determined based on RAIN analysis (Thaben and Westermark, 2014).

Differential rhythmicity analysis was performed on genes that met the criteria for rhythmicity on the datasets for both genotypes with DODR (Thaben and Westermark, 2016), using the following options: norm = FALSE, period = 24, method = "robust," verbose = options("verbose"). Genes were scored as differentially rhythmic between genotypes when the meta.p value, which is a corrected *p-value*, generated by the software was < 0.1.

Differential expression analysis—Both the circadian RNaseq and the fasted-refeeding RNaseq datasets were processed with edgeR (Robinson et al., 2010).

Circadian dataset genes were defined as differentially expressed between genotypes at q < 0.1.

Fasted and refed RNA-seq data genes we first defined food responsive genes for each genotype if q < 0.1 between their corresponding fasted and fed groups. Next, we selected genes that were food-responsive in normal livers but scored as non-responsive in the mutant background or that were scored as responsive in both and assessed whether their fold induction was equal or greater than a 30% change. Genes meeting these criteria were further analyzed by a performing a permutation test (5000 Monte Carlo simulations) between their fasted-normalized fed values, and those with a q < 0.1 were scored as differentially induced.

Pathway analysis—Circadian dataset analysis was performed with DAVID (Huang et al., 2009a, 2009b) to determine enriched Panther pathways with a p < 0.05 in which at least four genes were present. The food-induced gene set that was affected by JARID1a ablation was analyzed with Ingenuity Pathway Analysis software (QIAGEN) to determine canonical pathways and upstream regulator prediction. For the latter, we focused on transcription factors and ligand-regulated nuclear receptors sets and used an absolute z-score value of 1 with a p < 0.005, excluding any regulators that are not expressed in liver.

QUANTIFICATION AND STATISTICAL ANALYSIS

In all statistical analysis n denotes biological replicates with the specific number indicated in the corresponding Figure legends. Gene expression data for both circadian and fasted/re-feeding datasets are mean CPM ± s.e.m. normalized to the maximal value obtained in control genotype. Specific lipid metabolite graphed values represent mean+/− s.e.m. peak heights (mTIC) obrained from GC-TOF/MS, normalized to the highest value observed in control cohorts. Statistical analysis for the glucose, pyruvate and insulin tolerance tests were assessed with a repeated-measures two-way ANOVA. For all other analysis statistical comparisons were done with a permutation without replacement test (Monte Carlo simulations) done with a custom R script provided in Data S3. Multiple test corrections were performed via Benjamini-Hoesch method.

Rhythmicity, differential rhythmicity, and differential gene expression analysis were performed with MetaCycle, RAIN, DODR, and edgeR algorithms described in detail in the corresponding Method Details section

Supplementary Material

Refer to Web version on PubMed Central for supplementary material.

ACKNOWLEDGMENTS

We thank Shubhroz Gill and Partha Kasturi for comments and useful discussions, and the KUMC Laboratory Animal Resources, Metabolic Core, and the Department of Pharmacology Core. Mice strains are commercially available from Jackson Laboratory. The data presented in this report is found either in the main text or in the supplemental materials. RNA-seq data have been made available at NCBI's Sequence Read Archive. This work was supported by the National Institute of Diabetes and Digestive and Kidney Diseases under grant number R01DK108088 (to L.D.); the Lied Basic Science Program (to L.D.); the National Center for Research Resources (P20RR021940); the National Institute of General Medical Sciences P20GM103549 and P30GM118247 to the Department of Pharmacology, Toxicology, and Therapeutics; and the National Institutes of Health, Institutional Development Award (IDeA) from the National Institute of General Medical Sciences of the National Institutes of Health under grant number P20 GM103418. The Vanderbilt University Hormone Assay & Analytics Core and Lipid Core are supported by National Institute of Diabetes and Digestive and Kidney Diseases grants DK059637 and DK020593. West Coast Metabolomics at UC Davis is supported by NIH U2C ES030158 and 1U24DK097154. The IPA software used in this publication was supported by the Biostatistics and Informatics Shared Resource, funded by the National Cancer Institute Cancer Center Support Grant P30 CA168524, and the Kansas IDeA Network of Biomedical Research Excellence Bioinformatics Core, supported in part by the National Institute of General Medical Sciences award P20GM103418.

REFERENCES

Albrecht U (2012). Circadian rhythms and sleep–the metabolic connection. Pflugers Arch. 463, 23–30. [PubMed: 21710201]

Altarejos JY, and Montminy M (2011). CREB and the CRTC co-activators: sensors for hormonal and metabolic signals. Nat. Rev. Mol. Cell Biol 12, 141–151. [PubMed: 21346730]

Asada M, Rauch A, Shimizu H, Maruyama H, Miyaki S, Shibamori M, Kawasome H, Ishiyama H, Tuckermann J, and Asahara H (2011). DNA binding-dependent glucocorticoid receptor activity promotes adipogenesis via Krüppel-like factor 15 gene expression. Lab. Invest 91, 203–215. [PubMed: 20956975]

Bass J, and Takahashi JS (2010). Circadian integration of metabolism and energetics. Science 330, 1349–1354. [PubMed: 21127246]

Benegiamo G, Mure LS, Erikson G, Le HD, Moriggi E, Brown SA, and Panda S (2018). The RNA-binding protein NONO coordinates hepatic adaptation to feeding. Cell Metab. 27, 404–418 e407. [PubMed: 29358041]

Benevolenskaya EV, Murray HL, Branton P, Young RA, and Kaelin WG Jr. (2005). Binding of pRB to the PHD protein RBP2 promotes cellular differentiation. Mol. Cell 18, 623–635. [PubMed: 15949438]

Besseiche A, Riveline JP, Gautier JF, Bréant B, and Blondeau B (2015). Metabolic roles of PGC-1α and its implications for type 2 diabetes. Diabetes Metab. 41, 347–357. [PubMed: 25753246]

Chaix A, Zarrinpar A, Miu P, and Panda S (2014). Time-restricted feeding is a preventative and therapeutic intervention against diverse nutritional challenges. Cell Metab. 20, 991–1005. [PubMed: 25470547]

Chan SW, and Hong W (2001). Retinoblastoma-binding protein 2 (Rbp2) potentiates nuclear hormone receptor-mediated transcription. J. Biol. Chem 276, 28402–28412. [PubMed: 11358960]

Deng Y, Wang ZV, Tao C, Gao N, Holland WL, Ferdous A, Repa JJ, Liang G, Ye J, Lehrman MA, et al. (2013). The Xbp1s/GalE axis links ER stress to postprandial hepatic metabolism. J. Clin. Invest 123, 455–468. [PubMed: 23257357]

DiTacchio L, Le HD, Vollmers C, Hatori M, Witcher M, Secombe J, and Panda S (2011). Histone lysine demethylase JARID1a activates CLOCK-BMAL1 and influences the circadian clock. Science 333, 1881–1885. [PubMed: 21960634]

Dobin A, Davis CA, Schlesinger F, Drenkow J, Zaleski C, Jha S, Batut P, Chaisson M, and Gingeras TR (2013). STAR: ultrafast universal RNA-seq aligner. Bioinformatics 29, 15–21. [PubMed: 23104886]

Doi R, Oishi K, and Ishida N (2010). CLOCK regulates circadian rhythms of hepatic glycogen synthesis through transcriptional activation of Gys2. J. Biol. Chem 285, 22114–22121. [PubMed: 20430893]

Feng D, and Lazar MA (2012). Clocks, metabolism, and the epigenome. Mol. Cell 47, 158–167. [PubMed: 22841001]

Feng D, Liu T, Sun Z, Bugge A, Mullican SE, Alenghat T, Liu XS, and Lazar MA (2011). A circadian rhythm orchestrated by histone deacetylase 3 controls hepatic lipid metabolism. Science 331, 1315–1319. [PubMed: 21393543]

Green CB, Takahashi JS, and Bass J (2008). The meter of metabolism. Cell 134, 728–742. [PubMed: 18775307]

Greenwell BJ, Trott AJ, Beytebiere JR, Pao S, Bosley A, Beach E, Finegan P, Hernandez C, and Menet JS (2019). Rhythmic food intake drives rhythmic gene expression more potently than the hepatic circadian clock in mice. Cell Reports 27, 649–657 e645. [PubMed: 30995463]

Hatori M, Vollmers C, Zarrinpar A, DiTacchio L, Bushong EA, Gill S, Leblanc M, Chaix A, Joens M, Fitzpatrick JA, et al. (2012). Time-restricted feeding without reducing caloric intake prevents metabolic diseases in mice fed a high-fat diet. Cell Metab. 15, 848–860. [PubMed: 22608008]

Hayakawa T, Ohtani Y, Hayakawa N, Shinmyozu K, Saito M, Ishikawa F, and Nakayama J (2007). RBP2 is an MRG15 complex component and down-regulates intragenic histone H3 lysine 4 methylation. Genes Cells 12, 811–826. [PubMed: 17573780]

Herzig S, Long F, Jhala US, Hedrick S, Quinn R, Bauer A, Rudolph D, Schutz G, Yoon C, Puigserver P, et al. (2001). CREB regulates hepatic gluconeogenesis through the coactivator PGC-1. Nature 413, 179–183. [PubMed: 11557984]

Huang W, Sherman BT, and Lempicki RA (2009a). Bioinformatics enrichment tools: paths toward the comprehensive functional analysis of large gene lists. Nucleic Acids Res. 37, 1–13. [PubMed: 19033363]

Huang W, Sherman BT, and Lempicki RA (2009b). Systematic and integrative analysis of large gene lists using DAVID bioinformatics resources. Nat. Protoc 4, 44–57. [PubMed: 19131956]

Hughes ME, DiTacchio L, Hayes KR, Vollmers C, Pulivarthy S, Baggs JE, Panda S, and Hogenesch JB (2009). Harmonics of circadian gene transcription in mammals. PLoS Genet. 5, e1000442. [PubMed: 19343201]

Ishikawa K, and Shimazu T (1980). Circadian rhythm of liver glycogen metabolism in rats: effects of hypothalamic lesions. Am. J. Physiol 238, E21–E25. [PubMed: 6766673]

Jeyaraj D, Scheer FA, Ripperger JA, Haldar SM, Lu Y, Prosdocimo DA, Eapen SJ, Eapen BL, Cui Y, Mahabeleshwar GH, et al. (2012). Klf15 orchestrates circadian nitrogen homeostasis. Cell Metab. 15, 311–323. [PubMed: 22405069]

Kalvisa A, Siersbæk MS, Præstholm SM, Christensen LJL, Nielsen R, Stohr O, Vettorazzi S, Tuckermann J, White M, Mandrup S, and Grøntved L (2018). Insulin signaling and reduced glucocorticoid receptor activity attenuate postprandial gene expression in liver. PLoS Biol. 16, e2006249. [PubMed: 30532187]

Kohsaka A, Laposky AD, Ramsey KM, Estrada C, Joshu C, Kobayashi Y, Turek FW, and Bass J (2007). High-fat diet disrupts behavioral and molecular circadian rhythms in mice. Cell Metab. 6, 414–421. [PubMed: 17983587]

Koike N, Yoo S-H, Huang H-C, Kumar V, Lee C, Kim T-K, and Takahashi JS (2012). Transcriptional architecture and chromatin landscape of the core circadian clock in mammals. Science 338, 349–354. [PubMed: 22936566]

Lamia KA, Storch KF, and Weitz CJ (2008). Physiological significance of a peripheral tissue circadian clock. Proc. Natl. Acad. Sci. USA 105, 15172–15177. [PubMed: 18779586]

Lopez-Bigas N, Kisiel TA, Dewaal DC, Holmes KB, Volkert TL, Gupta S, Love J, Murray HL, Young RA, and Benevolenskaya EV (2008). Genome-wide analysis of the H3K4 histone demethylase RBP2 reveals a transcriptional program controlling differentiation. Mol. Cell 31, 520–530. [PubMed: 18722178]

Ma D, Panda S, and Lin JD (2011). Temporal orchestration of circadian autophagy rhythm by C/EBPβ. EMBO J. 30, 4642–4651. [PubMed: 21897364]

Mange F, Praz V, Migliavacca E, Willis IM, Schütz F, and Hernandez N; CycliX Consortium (2017). Diurnal regulation of RNA polymerase III transcription is under the control of both the feeding-fasting response and the circadian clock. Genome Res. 27, 973–984. [PubMed: 28341772]

Marcheva B, Ramsey KM, Buhr ED, Kobayashi Y, Su H, Ko CH, Ivanova G, Omura C, Mo S, Vitaterna MH, et al. (2010). Disruption of the clock components CLOCK and BMAL1 leads to hypoinsulinaemia and diabetes. Nature 466, 627–631. [PubMed: 20562852]

Panda S, Antoch MP, Miller BH, Su AI, Schook AB, Straume M, Schultz PG, Kay SA, Takahashi JS, and Hogenesch JB (2002). Coordinated transcription of key pathways in the mouse by the circadian clock. Cell 109, 307–320. [PubMed: 12015981]

Picelli S, Björklund AK, Faridani OR, Sagasser S, Winberg G, and Sandberg R (2013). Smart-seq2 for sensitive full-length transcriptome profiling in single cells. Nat. Methods 10, 1096–1098. [PubMed: 24056875]

Quiros PM, Goyal A, Jha P, and Auwerx J (2017). Analysis of mtDNA/ nDNA Ratio in Mice. Curr. Protoc. Mouse Biol 7, 47–54. [PubMed: 28252199]

Robinson MD, McCarthy DJ, and Smyth GK (2010). edgeR: a Bio-conductor package for differential expression analysis of digital gene expression data. Bioinformatics 26, 139–140. [PubMed: 19910308]

Rui L (2014). Energy metabolism in the liver. Compr. Physiol 4, 177–197. [PubMed: 24692138]

Schibler U, Ripperger J, and Brown SA (2003). Peripheral circadian oscillators in mammals: time and food. J. Biol. Rhythms 18, 250–260. [PubMed: 12828282]

Sokolović M, Sokolovic A, Wehkamp D, Ver Loren van Themaat E, de Waart DR, Gilhuijs-Pederson LA, Nikolsky Y, Kampen AH, Hakvoort TB, and Lamers WH (2008). The transcriptomic signature of fasting murine liver. BMC Genomics 9, 528. [PubMed: 18990241]

Solloway MJ, Madjidi A, Gu C, Eastham-Anderson J, Clarke HJ, Kljavin N, Zavala-Solorio J, Kates L, Friedman B, Brauer M, et al. (2015). Glucagon couples hepatic amino acid catabolism to mTOR-dependent regulation of α-cell mass. Cell Rep. 12, 495–510. [PubMed: 26166562]

Tahara Y, and Shibata S (2016). Circadian rhythms of liver physiology and disease: experimental and clinical evidence. Nat. Rev. Gastroenterol. Hepatol 13, 217–226. [PubMed: 26907879]

Takashima M, Ogawa W, Hayashi K, Inoue H, Kinoshita S, Okamoto Y, Sakaue H, Wataoka Y, Emi A, Senga Y, et al. (2010). Role of KLF15 in regulation of hepatic gluconeogenesis and metformin action. Diabetes 59, 1608–1615. [PubMed: 20393151]

Tempel DL, Shor-Posner G, Dwyer D, and Leibowitz SF (1989). Nocturnal patterns of macronutrient intake in freely feeding and food-deprived rats. Am. J. Physiol 256, R541–R548. [PubMed: 2916704]

Thaben PF, and Westermark PO (2014). Detecting rhythms in time series with RAIN. J. Biol. Rhythms 29, 391–400. [PubMed: 25326247]

Thaben PF, and Westermark PO (2016). Differential rhythmicity: detecting altered rhythmicity in biological data. Bioinformatics 32, 2800–2808. [PubMed: 27207944]

Tornatore L, Thotakura AK, Bennett J, Moretti M, and Franzoso G (2012). The nuclear factor kappa B signaling pathway: integrating metabolism with inflammation. Trends Cell Biol. 22, 557–566. [PubMed: 22995730]

Vollmers C, Gill S, DiTacchio L, Pulivarthy SR, Le HD, and Panda S (2009). Time of feeding and the intrinsic circadian clock drive rhythms in hepatic gene expression. Proc. Natl. Acad. Sci. USA 106, 21453–21458. [PubMed: 19940241]

Wu G, Anafi RC, Hughes ME, Kornacker K, and Hogenesch JB (2016). MetaCycle: an integrated R package to evaluate periodicity in large scale data. Bioinformatics 32, 3351–3353. [PubMed: 27378304]

Yeung J, Mermet J, Jouffe C, Marquis J, Charpagne A, Gachon F, and Naef F (2018). Transcription factor activity rhythms and tissue-specific chromatin interactions explain circadian gene expression across organs. Genome Res. 28, 182–191. [PubMed: 29254942]

Zhao LF, Iwasaki Y, Nishiyama M, Taguchi T, Tsugita M, Okazaki M, Nakayama S, Kambayashi M, Fujimoto S, Hashimoto K, et al. (2012). Liver X receptor α is involved in the transcriptional

regulation of the 6-phosphofructo-2-kinase/fructose-2,6-bisphosphatase gene. Diabetes 61, 1062–1071. [PubMed: 22415873]

Highlights

- Loss of hepatic JARID1a disrupts large-scale rhythms in transcription
- JARID1a is required for the hepatic transcriptomic food response
- Mice that lack liver JARID1a have defects in glucose, lipid, and amino acid metabolism

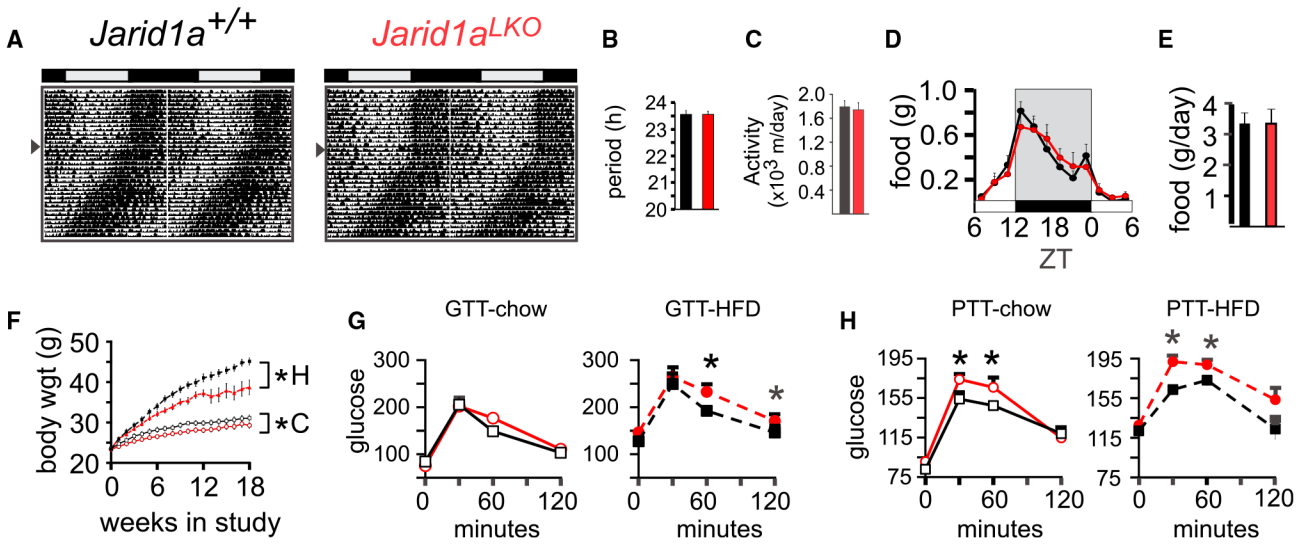

Figure 1. Metabolic Phenotype of *Jarid1a*^{LKO} Mice

(A) Representative circadian double-plotted diurnal and circadian activity of control and *Jarid1a*^{LKO} mice. All actograms obtained are shown in Figure S1A. (B) Circadian period length of the indicated cohorts (mean ± SEM, n = 3 mice). (C) Circadian period length of the total activity (distance traveled, mean ± SEM meters/day). (D and E) Diurnal profile (D) and total daily food consumption (E) for control and *Jarid1a*^{LKO} mice under 12 h:12 h light:dark cycle (mean ± SEM n = 6 mice/cohort). (F) Weight gain under regular or high-fat diets (HFDs) (mean ± SEM, control n = 19, *Jarid1a*^{LKO} n = 24). (G) Intraperitoneal glucose tolerance test (GTT) for mice under regular chow (control n = 10, *Jarid1a*^{LKO} n = 10) or a HFD (control n = 14 mice, *Jarid1a*^{LKO} n = 8 mice), glucose units are mg/dL. (H) Intraperitoneal pyruvate tolerance test (PTT) for mice under regular chow (control n = 14 mice, *Jarid1a*^{LKO} n = 11 mice) or a HFD (control n = 8 mice, *Jarid1a*^{LKO} n = 11 mice); glucose units are mg/dL. Data for (F)–(H) are presented as mean ± SEM. *p < 0.05, **p < 0.01; p values obtained in (E) with repeated-measures ANOVA, and (G) and (H) with permutation tests. Area under the curve for (G) and (H) presented in Figure S1B.

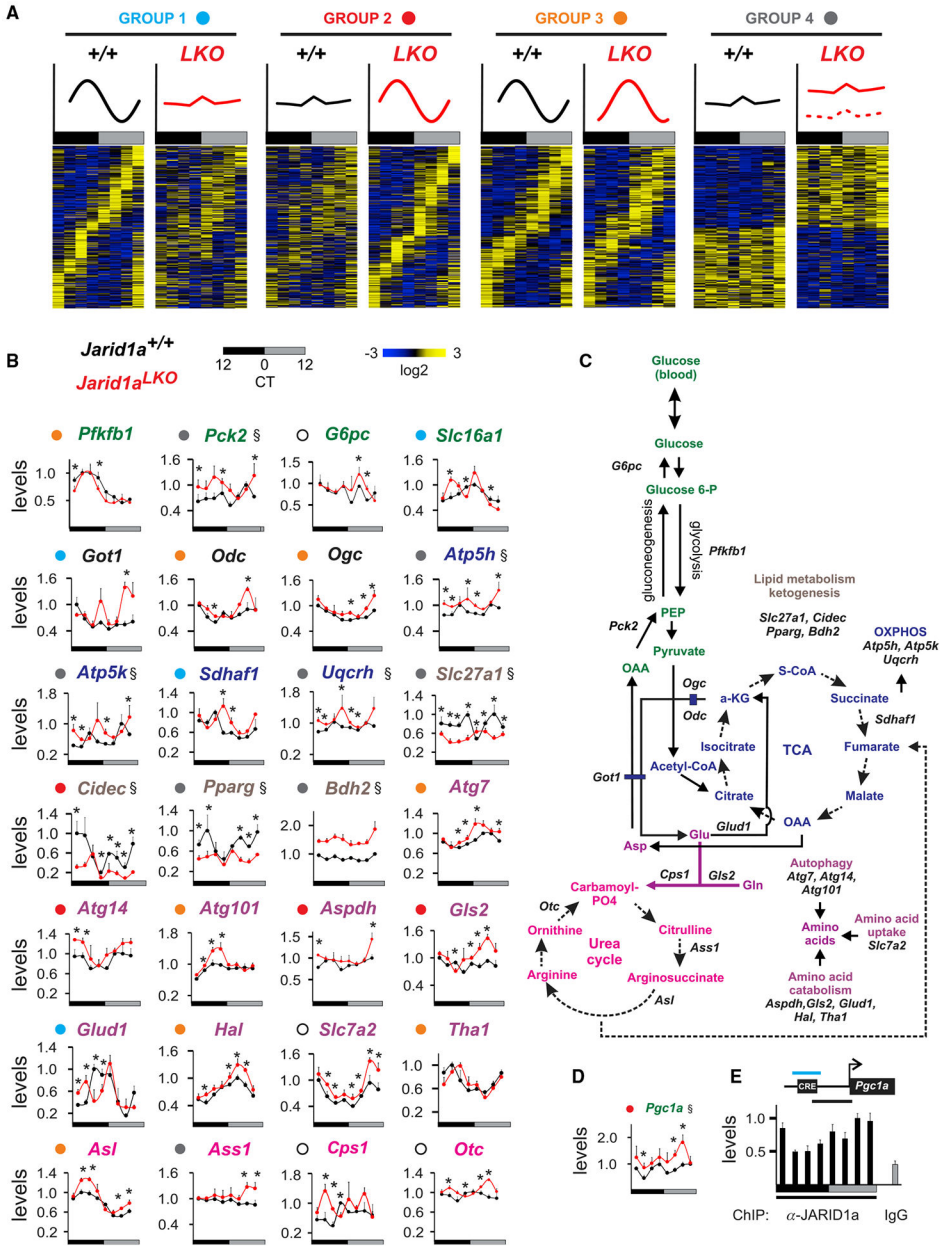

Figure 2. JARID1a Deficiency Perturbs the Hepatic Transcriptome

(A) Heatmaps of hepatic gene transcripts scored as rhythmic only in control (Group 1), rhythmic only in *Jarid1a*^{LKO} (Group 2), differentially rhythmic (Group 3) and differentially expressed non-circadian (Group 4), with top ontological terms shown in Figure S2C. Each row represents an individual transcript and each column the average of three biological replicates for each time point using log2-transformed mean-centered expression values. At the top of each heatmap we provide a graphical summary of each classification. (B) Time-resolved examples of genes impacted by JARID1a ablation (3-h resolution). Levels correspond to counts-per-million normalized to the maximum value of the indicated gene in control livers. Colored dots indicate the group classification of each specific gene shown, as indicated in (A). Open circles denote manually selected transcripts. Font color matches are

the same as given in (C). (C) Primary metabolic pathways and processes affected in *Jarid1a*^{LKO} livers. Carbohydrate (green), TCA cycle and oxidative phosphorylation (blue), fatty acid processes (brown), amino acid metabolism (purple), urea cycle (pink), and genes that overlap macronutrient pathways (black). (D) *Pgc1a* transcript levels in control and mutant livers. (E) JARID1a occupancy at the PGC1a gene promoter determined by chromatin immunoprecipitation (ChIP)-qPCR. Black box denotes a critical CRE box. Lower black bar region of RNA Pol II occupancy (Koike et al., 2012). Top blue bar denotes the amplified region. Levels correspond to % inputs normalized to maximal value. Data for (B), (D), and (E) are n = 3 biological replicates, mean ± SEM; *p < 0.05 and §p < 0.0*5*. p values were obtained by one-tailed permutation test.

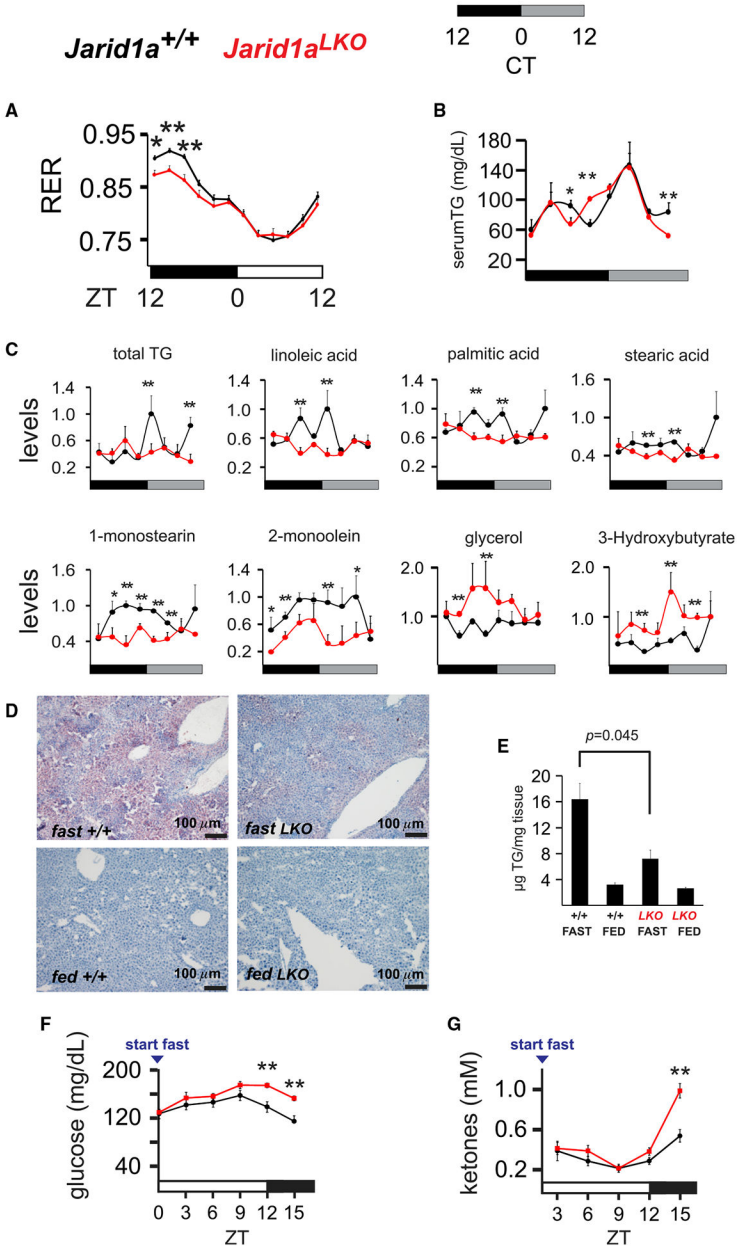

Figure 3. Increased Lipid Use in *Jarid1a*^{LKO} Mice and Livers

(A) Diurnal respiratory exchange ratio (RER); mean ± SEM, n = 10 mice. Black and white bars, dark-light cycle (dark starts at 18:00 h, light at 6:00 h). (B) Circadian serum triglycerides (TGs) of control and *Jarid1a*^{LKO} animals (mean ± SEM, n = 3). (C) Hepatic circadian profile of normalized levels for total TGs, with indicated fatty acids, glycerol, and β-hydroxybutyrate. TG levels represent values normalized to maximum concentration of the control timeline (12 μg/mg tissue). Specific lipid levels were obtained by GC-TOFMS and values correspond to total ion counts normalized to the maximal value obtained in control timeline. Data is shown as mean ± SEM, n = 3. (D) Representative Oil Red-O staining of liver sections from fasted or fed control and *Jarid1a*^{LKO} animals at 10x magnification. (E) TG quantification for livers used in (D) (mean ± SEM, n = 5 mice per control cohort and n =

4 per mutant cohorts). (F and G) Blood glucose (F) and ketone (G) levels of mice subjected to fasting (mean ± SEM, n = 8). $p < 0.05$, $^{**}p < 0.01$. Statistical data determined with a one-tailed permutation test.

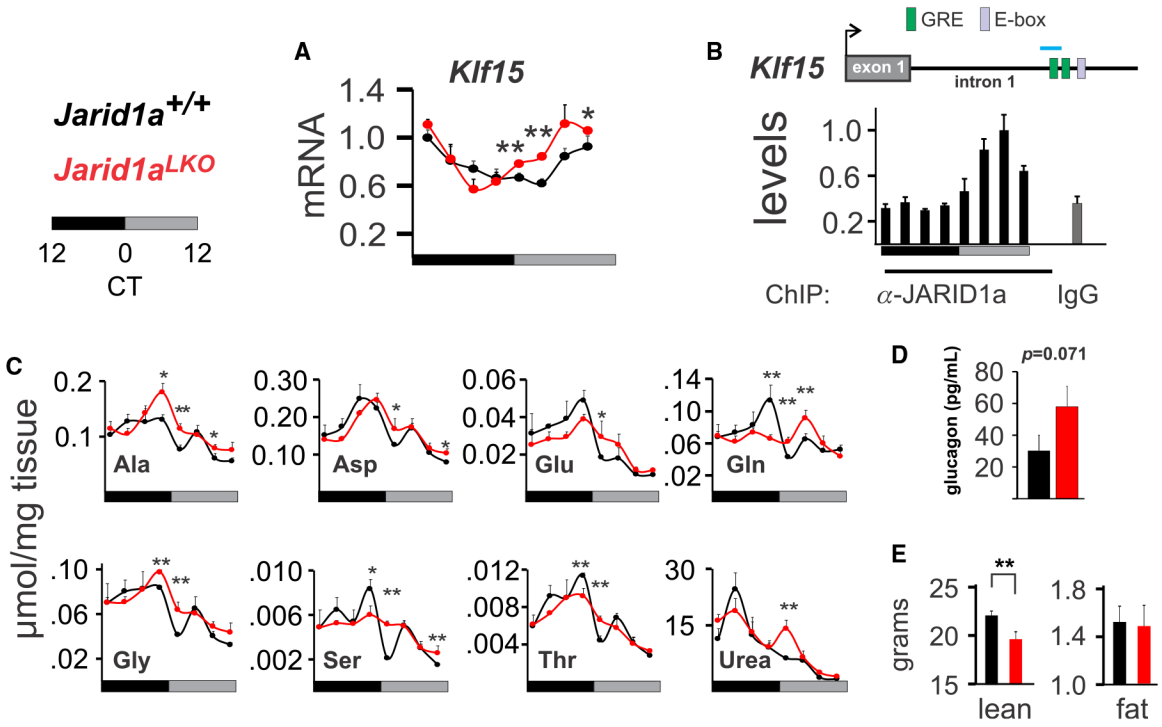

Figure 4. *Jarid1a*^{LKO} Livers Exhibit Abnormal Amino Acid Metabolism

(A) The circadian profile of *Klf15* mRNA is altered in JARID1a deficient livers (mean ± SEM, n = 3 biological replicates per time point, **p < 0.01). (B) ChIPs performed with an anti-JARID1a antibody or immunoglobulin (IgG) from control or *Jarid1a*^{LKO} mouse liver chromatin. α-JARID1a ChIPs were performed across the circadian cycle (mean ± SEM, n = 3 biological replicates) in normal chromatin. IgG from control and JARID1a from JARID1a-null chromatin are averages of a circadian timeline (n = 8 biological replicates for both). Shown are mean ± SEM of levels normalized % input to the maximal levels of JARID1a occupancy (2%). Glucocorticoid response element (GRE) and E-box locations in the first introns are indicated as boxes; top blue bar denotes the amplified region. (C) Hepatic content of gluconeogenic amino acids in control and mutant livers across the circadian cycle (mean ± SEM, n = 3 biological replicates). (D) Plasma glucagon levels of control and *Jarid1a*^{LKO} mice fasted for 24 h (mean ± SEM, n = 6 control and n = 9 mutant biological replicates). (E) Total lean and fat body content from control and hepatic JARID1a-null animals (mean ± SEM, n = 8 control, n = 6 animals). *p < 0.05, **p < 0.01. Statistical data determined with a one-tailed permutation test.

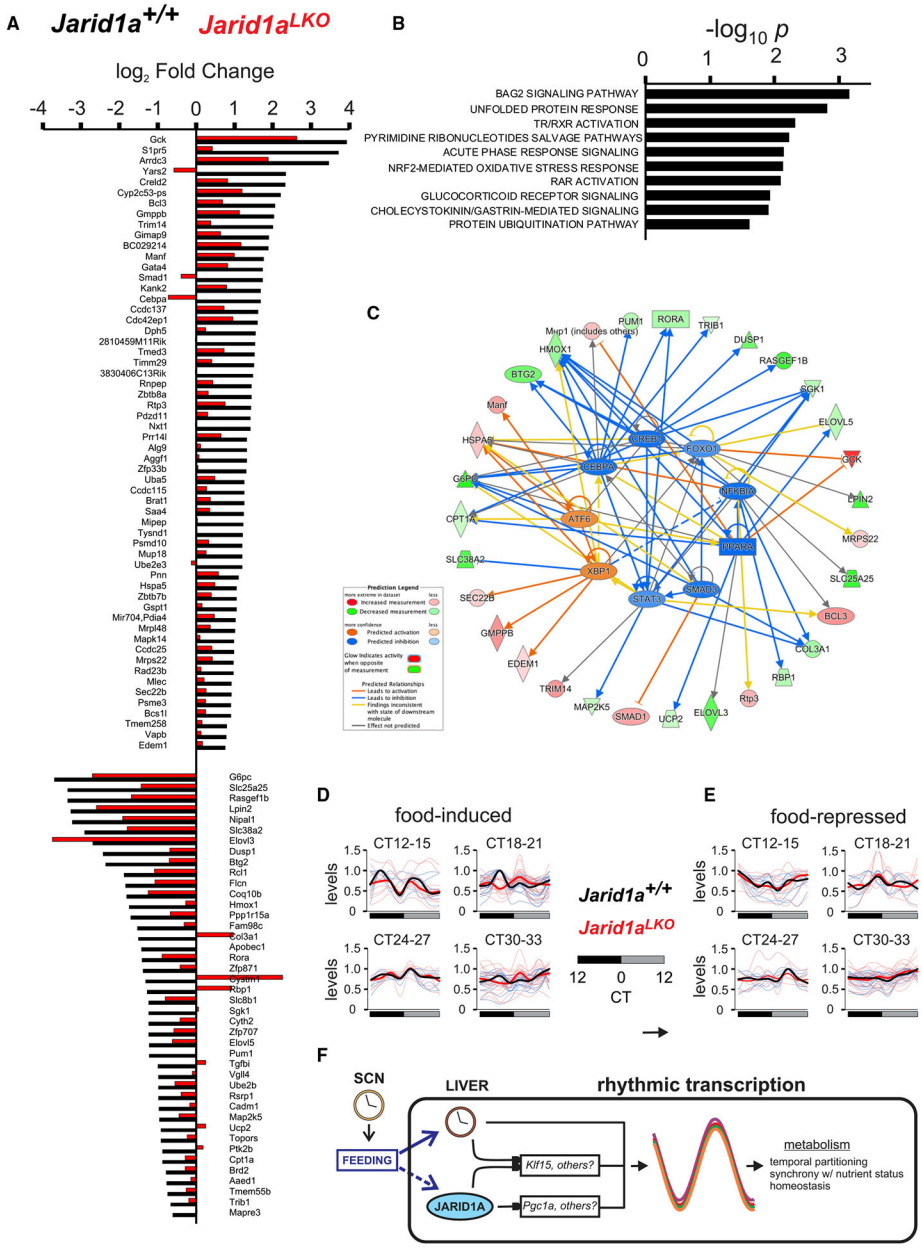

Figure 5. JARID1a-Null Livers Show Defective Transcriptional Response to Nutrient Availability

(A) Food-induced and repressed genes impacted by absence of *Jarid1a*. Shown is fold activation from baseline levels following food consumption. (B) Enriched canonical pathways of the gene set affected by ablation of *Jarid1a* livers. (C) Ingenuity Pathway Analysis predicted upstream transcriptional regulators of the gene set shown in (A) and (B). (D and E) Profile of food-induced (D) and food-repressed genes (E) affected in *Jarid1a*^{LKO} livers in control and JARID1a-null circadian timeline. The median of normalized expression levels of each group of transcripts in control (black) and *Jarid1a*^{LKO} (red) timeline is superimposed over the profiles of the individual transcripts in both genotypes (light blue and

light pink). (F) Model depicting how JARID1a participates in the maintenance of large-scale rhythms in transcription.

KEY RESOURCES TABLE

REAGENT or RESOURCE	SOURCE	IDENTIFIER
Antibodies		
Anti-ACC	Cell Signaling Technologies	Cat#3676P; RRID:AB_2219397
Anti-phospho ACC	Cell Signaling Technologies	Cat#3661P; RRID:AB_330337
Anti-mTOR	Cell Signaling Technologies	Cat#2983S; RRID:AB_2105622
Anti-phospho mTOR	Cell Signaling Technologies	Cat#5536S; RRID:AB_10691552
Control rabbit IgG	Bethyl Laboratories	P120–101
Anti-JARID1a	This paper	RRID:AB_2847888
Chemicals, Peptides, and Recombinant Proteins		
EGS (ethylene glycol bis(succinimidyl succinate))	Thermo Fisher Scientific	Cat#21565
complete protease inhibitor	Millipore Sigma	Cat#11697498001
PhosSTOP phosphatase inhibitor	Millipore Sigma	Cat#4906845001
Critical Commercial Assays		
Pierce BCA Assay Kit	Thermo Fisher Scientific	Cat#23225
Triglyceride assay kit	Pointe Scientific, Inc	Cat#T732–500
Glucagon ELISA kit, Chemoluminescent	Millipore Sigma	Cat#EZGLU-30K
Deposited Data		
Circadian timeline RNA-sequencing data of control and Jarid1a^{LKO} mice	This paper	SRA PRJNA626351
RNA-sequencing data for fasted and re-fed control and Jarid1a^{LKO} mice	This paper	SRA PRJNA626368
Experimental Models: Organisms/Strains		
Mouse: B6.129S6(Cg)-Kdm5atm1Kael/J	The Jackson Laboratory	stock 008572
Mouse: B6.Cg-Speer6-ps1Tg(Alb-cre)21 Mgn/J	The Jackson Laboratory	stock 003574
Oligonucleotides		
Klf15 intron-Fwd, 5’-CCT ACA GGT GCG AGA ATG GCA G-3’	This publication	N/A
mKlf 15 in-Rev, 5’-CAG GCC TGC TGT TTA TCC TC-3’	This publication	N/A
Pgda Pro-Fwd, 5’-CAG AGG GCT GCC TTG GA-3’	This publication	N/A
Pgda Pro-Rev, 5’-CAG CCT CCC TTC TCC TGT G-3’	This publication	N/A
Hk2-Fwd: 5’-GCC AGC CTC TCC TGA TTT TAG TGT-3’	Quiros et al., 2017	N/A
Hk2Rev: 5’-GGG AAC ACA AAA GAC CTC TTC TGG-3’	Quiros et al., 2017	N/A
ND1 -Fwd, 5’-CTA GCA GAA ACA AAC CGG GC-3’	Quiros et al., 2017	N/A

REAGENT or RESOURCE	SOURCE	IDENTIFIER
ND1 -Rev, 5'-CCG GCT GCG TAT TCT ACG TT-3'	Quiros et al., 2017	N/A
Software and Algorithms		
ClockLab	Actimetrics (Wilmette, IL, USA)	https://www.actimetrics.com/products/big-brother/
BigBrother	Actimetrics (Wilmette, IL, USA)	https://www.actimetrics.com/products/clocklab/
STAR Aligner	Dobin et al., 2013	https://github.com/alexdobin/STAR
MetaCycle	Wu et al., 2016	https://github.com/gangwug/MetaCycle
RAIN	Thaben and Westermark, 2014	https://www.bioconductor.org/packages/release/bioc/html/rain.html
DODR	Thaben and Westermark, 2016	https://cran.r-project.org/web/packages/DODR/index.html
edgeR	Robinson et al., 2010	https://bioconductor.org/packages/release/bioc/html/edgeR.html
Permutation test R script	This publication	N/A
Other		
PerfeCTa SYBR Green FastMix	Quanta bio	Cat#95072–05K
Dynabeads (Protein G)	Thermo Fisher Scientific	Cat#10004D
NovaMax Plus Blood Glucose and Ketone Meter	Nova Diabetics Care/Nova Biomedical	N/A
FreeStyle Lite Glucose Meter	Abott	N/A
High-fat diet (42% calories from fat)	ENVIGO (Tekla Custom Diets)	TD.88137